

# Journal Pre-proof

Influence of age-related bone density changes on primary stability in stemless shoulder arthroplasty: A multi-implant finite element study

Helena L. Monteiro, Madalena Antunes, Marco Sarmento, Carlos Quental, João Folgado

PII: S1058-2746(24)00403-8

DOI: <https://doi.org/10.1016/j.jse.2024.04.013>

Reference: YMSE 6865

To appear in: *Journal of Shoulder and Elbow Surgery*

Received Date: 8 January 2024

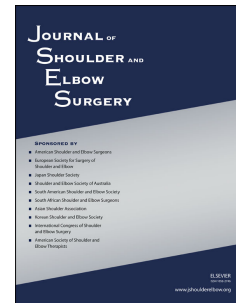
Revised Date: 2 April 2024

Accepted Date: 8 April 2024

Please cite this article as: Monteiro HL, Antunes M, Sarmento M, Quental C, Folgado J, Influence of age-related bone density changes on primary stability in stemless shoulder arthroplasty: A multi-implant finite element study, *Journal of Shoulder and Elbow Surgery* (2024), doi: <https://doi.org/10.1016/j.jse.2024.04.013>.

This is a PDF file of an article that has undergone enhancements after acceptance, such as the addition of a cover page and metadata, and formatting for readability, but it is not yet the definitive version of record. This version will undergo additional copyediting, typesetting and review before it is published in its final form, but we are providing this version to give early visibility of the article. Please note that, during the production process, errors may be discovered which could affect the content, and all legal disclaimers that apply to the journal pertain.

© 2024 Published by Elsevier Inc. on behalf of Journal of Shoulder and Elbow Surgery Board of Trustees.



**Title:** Influence of age-related bone density changes on primary stability in stemless shoulder arthroplasty: A multi-implant finite element study

**Running-title:** Stemless shoulder arthroplasty: aging and stability

1. **Helena L. Monteiro<sup>a</sup>** (L. Monteiro is the author's family name; Helena is the author's given name)

<sup>a</sup>IDMEC, Instituto Superior Técnico, Universidade de Lisboa, Lisbon, Portugal

Address: IDMEC, Instituto Superior Técnico, Universidade de Lisboa, Av. Rovisco Pais, 1 1049-001

Email: [helena.monteiro@tecnico.ulisboa.pt](mailto:helena.monteiro@tecnico.ulisboa.pt)

2. **Madalena Antunes<sup>a</sup>** (Antunes is the author's family name; Madalena is the author's given name)

<sup>a</sup>IDMEC, Instituto Superior Técnico, Universidade de Lisboa, Lisbon, Portugal

Address: IDMEC, Instituto Superior Técnico, Universidade de Lisboa, Av. Rovisco Pais, 1 1049-001

Email: [madalena.antunes@tecnico.ulisboa.pt](mailto:madalena.antunes@tecnico.ulisboa.pt)

ORCID-ID: 0000-0001-6736-4800

3. **Marco Sarmento<sup>b</sup>** (Sarmento is the author's family name; Marco is the author's given name)

<sup>b</sup>Hospital CUF Descobertas, Lisbon, Portugal

Address: R. Mário Botas, 1998-018 Lisboa

Email: [msarmento@medicina.ulisboa.pt](mailto:msarmento@medicina.ulisboa.pt)

ORCID-ID: 0000-0003-0550-6417

4. **Carlos Quental<sup>a,\*</sup>** (Quental is the author's family name; Carlos is the author's given name)

<sup>a</sup>IDMEC, Instituto Superior Técnico, Universidade de Lisboa, Lisbon, Portugal

*\* Corresponding author*

Address: IDMEC, Instituto Superior Técnico, Universidade de Lisboa, Av. Rovisco Pais, 1 1049-001

Email: [carlos.quental@tecnico.ulisboa.pt](mailto:carlos.quental@tecnico.ulisboa.pt)

ORCID-ID: 0000-0001-9034-8956

5. **João Folgado<sup>a</sup>** (Folgado is the author's family name; João is the author's given name)

<sup>a</sup>IDMEC, Instituto Superior Técnico, Universidade de Lisboa, Lisbon, Portugal

Address: IDMEC, Instituto Superior Técnico, Universidade de Lisboa, Av. Rovisco Pais, 1 1049-001

Email: [jfolgado@tecnico.ulisboa.pt](mailto:jfolgado@tecnico.ulisboa.pt)

ORCID-ID: 0000-0003-1160-7302

**Corresponding author:** Carlos Quental<sup>a,\*</sup> (Quental is the author's family name; Carlos is the author's given name)

<sup>a</sup>IDMEC, Instituto Superior Técnico, Universidade de Lisboa, Lisbon, Portugal

*\* Corresponding author*

Address: IDMEC, Instituto Superior Técnico, Universidade de Lisboa, Av. Rovisco Pais, 1 1049-001

Email: [carlos.quental@tecnico.ulisboa.pt](mailto:carlos.quental@tecnico.ulisboa.pt)

ORCID-ID: 0000-0001-9034-8956

Institutional review board approval was not required as this work is derived from anonymized data.

**Acknowledgments:** The authors acknowledge Fundação para a Ciência e a Tecnologia (FCT) for its financial support via the project LAETA Base Funding (DOI: 10.54499/UIDB/50022/2020) and the PhD scholarship 2021.06844.BD. The authors express gratitude to the Free Access Decedent Database, funded by the National Institute of Justice grant number 2016-DN-BX-0144, for providing the whole human body computed tomography (CT) scans that were instrumental in enabling this study.

#### **Disclaimers:**

**Funding:** This study received support from Fundação para a Ciência e a Tecnologia (FCT) via the project LAETA Base Funding and the PhD scholarship 2021.06844.BD.

Conflicts of interest: The authors, their immediate families, and any research foundation with which they are affiliated have not received any financial payments or other benefits from any commercial entity related to the subject of this article.

**Declaration of generative AI and AI-assisted technologies in the writing process**

During the preparation of this work the author(s) used ChatGPT in order to improve language and readability. After using this tool/service, the author(s) reviewed and edited the content as needed and take(s) full responsibility for the content of the publication.

## Abstract

**Background:** Stemless implants were introduced to prevent some of the stem-related complications associated with the total shoulder arthroplasty. Although general requirements for receiving these implants include good bone quality conditions, little knowledge exists about how bone quality affects implant performance. The goal of this study was to evaluate the influence of age-induced changes in bone density, as a metric of bone quality, in the primary stability of five anatomic stemless shoulder implants using 3D finite element (FE) models.

**Methods:** The implant designs considered were based on the Global Icon, Sidus, Simpliciti, SMR, and Inhance stemless implants. Shoulder arthroplasties were virtually simulated in Solidworks. The density distributions of 20 subjects from two age groups, 20 to 40 and 60 to 80 years old, were retrieved from medical image data and integrated into three-dimensional FE models of a single humerus geometry, developed in Abaqus, to avoid confounding factors associated with geometric characteristics. For the designs which do not have a solid collar covering the entire bone surface, i.e., the Sidus, Simpliciti, SMR, and Inhance implants, contact and non-contact conditions between the humeral head component and bone were considered. Primary stability was evaluated through the assessment of micromotions at the bone-implant interface considering eight load cases related to rehabilitation activities and demanding tasks. Three research variables, considering 20  $\mu\text{m}$ , 50  $\mu\text{m}$ , and 150  $\mu\text{m}$  as thresholds for osseointegration, were used for a statistical analysis of the results.

**Results:** The decreased bone density registered for the 60-80 age group led to larger micromotions at the bone-implant interface when compared to the 20-40 age group. The Global Icon-based and Inhance-based designs were the least sensitive to bone density, whereas the Sidus-based design was the most sensitive to bone density. The establishment of contact between the humeral head component and bone for the implants that do not have a solid collar led to decreased micromotions.

**Discussion:** Although the age-induced decline in bone density led to increased micromotions in the FE models, some stemless shoulder implants presented good overall performance regardless of the osseointegration threshold considered, suggesting that age alone may not be a contraindication to anatomic total shoulder arthroplasty. If only primary stability is considered, the results suggested superior performance for the Global Icon-based and Inhance-based designs. Moreover, the humeral head component should contact the resected bone surface when feasible. Further investigation is necessary to combine these results with the long-term performance of the implants and allow more precise recommendations.

**Level of Evidence:** Basic Science Study; Computer Modeling

**Keywords:** Shoulder arthroplasty; stemless shoulder implants; primary stability; micromotions; bone density; finite element method.

In an effort to recover shoulder function and reduce pain, the Anatomic Total Shoulder Arthroplasty (ATSA) replaces the humeral head and glenoid surfaces.<sup>13,40</sup> The loss of proximal humeral bone as a result of stress shielding, which raises the possibility of implant failure and periprosthetic fractures, is one of the most critical complications of ATSA.<sup>7</sup> The fourth generation of shoulder implants, known as stemless implants, represents the culmination of a pattern of progressive stem shortening to prevent some of the stem-related complications and reduce stress shielding.<sup>40</sup> Implant fixation is obtained through direct contact with the resected surface of metaphyseal bone, preserving more bone stock than the stemmed humeral components, which is critical for a possible revision surgery. Advantages of this last implant generation also include elimination of diaphyseal

stress concentrations, decreased risk of periprosthetic fractures, better shoulder anatomy recreation, simpler surgical technique, and less intraoperative blood loss.<sup>28,6,40</sup> Short-term, midterm, and long-term follow-up reports addressing the performance of stemless implants have shown promising functional and radiological results, comparable to those of traditional stemmed implants.<sup>21,1,20</sup>

The long-term success of stemless shoulder implants is sustained by the occurrence of osseointegration, which is only possible with adequate primary stability. Considering both the reliance on a shorter interaction surface for fixation and the support provided by a less stiff cancellous bone, stemless implants are more vulnerable from the stability point of view than stemmed implants.<sup>14,40</sup> Manufacturers recommend the use of these implants only when good bone quality is ensured<sup>10,11,26,41,44</sup>; however, no clear definition exists in the literature for good bone quality.<sup>17,9</sup> Given the correlation between aging and a deterioration in proximal humeral bone health<sup>33</sup>, a legitimate concern regarding their suitability for elderly patients arises.<sup>28</sup>

In vitro<sup>15</sup> and in silico<sup>14,31</sup> studies have investigated the primary stability of stemless implants, demonstrating an association between bone-implant micromotions and bone density, considered an indicator of bone quality.<sup>43,25</sup> While these studies provided valuable insights into the primary stability of stemless implants, some limitations constrained the scope of their conclusions. Favre and Henderson<sup>14</sup> and Favre et al<sup>15</sup> analyzed only one stemless implant (the Sidus Stem-Free Shoulder by Biomet), whose data should not be extrapolated to other stemless implants given their high geometric variability. Quental et al<sup>31</sup> analyzed five stemless implants but considered only homogeneous material properties. Considering the prevalence of complications in stemless shoulder arthroplasty and the existing knowledge gap on the impact of bone quality on the performance of stemless shoulder implants, the aim of this study was to investigate how changes in bone density due to aging affect the primary stability of five anatomic stemless shoulder

implants. For this purpose, three-dimensional (3D) finite element (FE) models incorporating heterogeneous bone density distributions, estimated from a cohort of subjects, were developed.

## Materials and Methods

This study presents a computational biomechanical analysis on the primary stability of 5 stemless shoulder implants using FE modeling. To avoid confounding factors associated with geometric characteristics, and to allow a direct comparison of results, all FE models of the stemless shoulder arthroplasties considered were based on a single 3D geometry of a right humerus, reconstructed from computed tomography (CT) scan images provided by the Visible Human Project<sup>36</sup>. Inter-subject bone quality variability was considered through the integration of distinct heterogeneous bone density distributions into this single right humerus geometry. The following sections provide further detail on the development of the baseline FE models of the stemless shoulder arthroplasties, built based on the studies of Comenda et al<sup>8</sup> and Quental et al<sup>31</sup>, and their adaptation for the simulation of different bone density distributions estimated from the CT data of a cohort of subjects.

### Finite element modeling

Five stemless implants, chosen to incorporate geometric variability while also considering global availability from manufacturers, were modeled in Solidworks (Dassault Systèmes, Waltham, MA, USA). The selected implants, exclusively focused on those fixed through impaction, include the Global Icon Stemless Shoulder System (DePuy Synthes, Warsaw, IN, USA), Sidus Stem-Free Shoulder (Biomet, Warsaw, IN, USA), Simpliciti Shoulder System (Wright Medical, formerly Tornier, Edina, MN, USA), SMR Stemless (Lima Corporate, San Daniele del Friuli, Italy), and Inhance Shoulder System (DePuy Synthes, Warsaw, IN, USA). For the sake of conciseness, these



implants are here on after referred to as “Global Icon-based”, “Sidus-based”, “Simpliciti-based”, “SMR-based”, and “Inhance-based”, respectively. The virtual simulation of the ATSAs, depicted in Figure 1, was performed in Solidworks, following the recommendations available on the surgical guides.<sup>10,11,26,41,44</sup>

Finite element models of the five stemless ATSAs were developed in Abaqus 2017 (Dassault Systèmes, Waltham, MA, USA) using linear tetrahedral (C3D4) elements. An average element size of 0.5 mm was assigned to the proximal humerus and metaphyseal components of the implants, as they represent the regions of greatest interest. For the humeral head component of the stemless implants and the humeral diaphysis, average element sizes of 1.8 mm and 2 mm were assigned, respectively. These dimensions were considered based on the findings of Quental et al<sup>31</sup>, who found them suitable through a sensitivity analysis. Bone was modeled as a heterogeneous linear elastic and isotropic material, with a Poisson’s ratio of 0.3 and Young’s modulus  $E$  as a function of bone apparent density  $\rho$ , given by:<sup>24</sup>

$$E \text{ (GPa)} = 2.61 \times \rho^{2.58} \quad (1)$$

The lower and upper density limits established for the application of Equation (1) were 0.048 g/cm<sup>3</sup> and 2.068 g/cm<sup>3</sup>, respectively. The minimum density was defined based on Keller<sup>24</sup>, while the maximum density was set to guarantee a Young's modulus of approximately 17 GPa for cortical bone, as considered by Favre et al<sup>14</sup>. All implant components were assumed linear elastic, homogeneous and isotropic materials, with a Poisson’s ratio of 0.3. A cobalt chromium alloy with a Young's modulus of 230 GPa was assigned to the humeral head component of each implant, while a titanium alloy with a Young's modulus of 115 GPa was assigned to the remaining implant components. A shell with a thickness of 0.5 mm and a Young's modulus of 17 GPa was modeled to simulate the outer cortical layer of the humerus.<sup>19,31</sup>

The interactions between bone and the stemless implants were modeled through a surface-to-surface contact formulation with friction. The friction coefficients considered for each interaction are summarized in Table I.<sup>31</sup> For implants that do not have a collar covering the entire bone surface, i.e., the Sidus, Simpliciti, SMR, and Inhance designs, the humeral head component can contact the bone surface. Given the challenge of achieving perfect placement *in vivo*, contact and non-contact conditions between bone and the humeral head components were simulated for these designs at the surfaces highlighted in red in Figure 1. The solid collar of the Global Icon design guarantees that no contact exists between its humeral head component and bone. The shell and bone were assumed to be rigidly connected using a tie constraint.

The orthoload database was used to obtain the *in vivo* glenohumeral joint forces and moments.<sup>4</sup> A total of eight load cases related to rehabilitation activities and demanding tasks were considered.<sup>31</sup> These included: 45° and 90° abduction motions with a 2 kg weight; 90° and 150° flexion motions with a 2 kg weight; lifting a coffee pot; nailing over the head level; turning a steering wheel with one hand; and putting a 2 kg weight on a shelf at head height. The center of the humeral head component was used as the application point for the glenohumeral joint forces and moments. Using coupling constraints, these joint forces and moments were distributed to the humeral head surface nodes nearest to the projection of the joint force onto the surface. A fully constrained (encastre) condition was imposed at the base of the humerus to prevent rigid body motion.<sup>8,14,31</sup>

### **Subject-specific bone density incorporation**

To investigate the influence of aging-induced changes in bone density on the primary stability of stemless implants, subject-specific bone densities were estimated within a selected population and were mapped into the 3D geometry of the humerus considered in the baseline FE models.<sup>35</sup> By employing a single 3D geometry of the humerus instead of a variety of geometries, bone density

became the only distinctive feature among subjects, which simplified result interpretation by excluding confounding factors, such as bone shape and size. The population selected for this study was divided into three age groups: 20 to 40, 40 to 60, and 60 to 80 years old. These groups are here on after referred to as “20-40”, “40-60”, and “60-80” age groups, respectively. Ten subjects were randomly selected for each age group from a population of over 200 subjects, collected from the New Mexico Decedent Image Database.<sup>12</sup>

For each subject, the 3D geometry of the right humerus was segmented from CT data using open-source software (e.g., ITK-SNAP<sup>42</sup> and 3D Slicer<sup>16</sup>). Using TetGen<sup>34</sup>, a volumetric mesh was generated for the reconstructed humerus geometry, and bone densities were estimated by establishing a linear relationship between bone density and Hounsfield units. A calibration procedure considering air and adipose tissue as calibration tissues was followed.<sup>2,39</sup> To map the bone density distribution of each subject’s humerus to the intact humerus geometry (i.e., before the simulation of the stemless shoulder arthroplasties) of the baseline FE models, elastic registration was performed, using the Coherence Point Drift algorithm<sup>29</sup>, to establish correspondence between the different volumetric mesh nodes.<sup>35</sup> An in-house code, developed in Matlab, was used to map the bone densities from the intact humerus geometry to the implanted FE meshes.

### **Evaluation of primary stability**

For each subject included in this study, nine FE analyses were performed, including all five stemless ATSAs modeled and the contact and non-contact conditions between bone and the humeral head components considered for the Sidus-based, Simpliciti-based, SMR-based, and Inhance-based implants. Micromotions at the bone-implant interface for the coated and blasted regions of the different stemless designs were used for the assessment of primary stability, as considered in previous studies.<sup>22,14,31</sup> By subtracting the displacement of an implant node from the

displacement of the corresponding bone node, micromotions were retrieved from the simulation as the relative motion between the implant and bone. Since bone and implant meshes did not match at the interface, interpolation was performed using the finite element shape functions. The highest micromotions predicted for each bone node among all load cases were assigned to each node in order to assess the worst-case scenario.<sup>31</sup>

## Statistical Analysis

With the aim of identifying the characteristics that statistically differentiated the three age groups, unpaired t-tests were conducted for mean bone density, weight, height, and bone mass index (BMI). Subsequently, three research variables were defined for the evaluation and comparison of the stemless implants' primary stability. These variables were based on the thresholds considered in the literature above which osseointegration is compromised.<sup>22,14,31,38</sup> Considering the lack of consensus in the literature regarding this threshold, the two extreme thresholds found, of 20  $\mu\text{m}$  and 150  $\mu\text{m}$ , were considered to account for worst- and best-case scenarios, respectively. Given the high difference between these thresholds and the values found in the literature<sup>22,38</sup>, an intermediate threshold of 50  $\mu\text{m}$  was also considered. Each research variable was defined as the percentage of coated or blasted area above the respective micromotion threshold, normalized by the total coated or blasted area of the implant, signifying the proportion of the coated or blasted area of the implant where osseointegration and, consequently, primary stability, may be at risk.

IBM SPSS Statistics (IBM Corp., Armonk, NY, USA) was used to test correlations between the defined research variables and age, age group, gender, and BMI. Preliminary results showed a positive correlation with the age group ( $p < 0.001$ ), which reinforced the need of this study and

strengthened the following statistical tests. To assess the significance of the differences found in the data, comparison tests between groups were conducted. Each of the research variables was compared between implants and head contact conditions through one-way analysis of variance (ANOVA) and post-hoc Tukey's multiple comparison tests.<sup>23,38</sup> These tests were performed in Matlab R2022b, using the functions *anova1* and *multcompare*. A significance level of 5% ( $p < 0.05$ ) was considered. For  $P$  values below .05, the null hypothesis was rejected, meaning that the difference between the means was considered statistically significant. The normality of the research variables was assessed before these tests. According to the Kolmogorov-Smirnov test, the groups were normally distributed.

## Results

Table II presents the subjects' demographics. The unpaired t-tests performed for average bone density, weight, height, and BMI between the three age groups showed only statistically significant differences in terms of bone density between the 20-40 and 40-60 age groups ( $p < 0.001$ ), and the 20-40 and 60-80 age groups ( $p < 0.001$ ). The difference in average bone density between the 40-60 and 60-80 age groups was not statistically significant ( $p = 1.000$ ). Therefore, for the sake of brevity, the 40-60 age group was discarded from this study, and only the 20-40 and 60-80 age groups were analyzed. For the interest reader, the supplementary material presents detailed  $P$  values from the unpaired t-tests comparing age groups (Table SI), along with the average bone density distributions of the 20-40 and 60-80 age groups (Figure S1). A general decrease in bone density was observed in the 60-80 age group when compared to the 20-40 age group, being especially evident in the central regions of the bone and below the anatomical neck level.

Figure 2 presents, for each age group, the average cumulative distributions of the coated or blasted surface areas with micromotions above a given value, normalized by the total coated or blasted surface area of each implant. For each coordinate pair, the y-coordinate represents the average percentage of coated or blasted area presenting micromotions equal to or greater than the micromotion given by the x-coordinate. For each implant, the normalized surface area was calculated as an average of the normalized surface areas computed for all 10 subjects included in each age group. The results dispersion in each age group, and for each implant, including mean and SD, is provided in the supplementary material (Figure S2). Micromotions were larger for the 60-80 age group than the 20-40 age group. The highest micromotions were mainly observed in the antero-superior region, as illustrated in Figure 3 for the average micromotion distributions of each age group. The largest peak micromotions occurred for the Simpliciti-based, Sidus-based, and SMR-based implants with no head contact.

The threshold of 150  $\mu\text{m}$ , considered in one of the three defined research variables, was only exceeded by two subjects, and only for the Simpliciti-based implant with no head contact. Consequently, no relevant data existed for a statistical analysis of this research variable. Figure 4 presents the multiple comparison tests performed to assess the significance of differences between groups considering osseointegration thresholds of 20  $\mu\text{m}$  and 50  $\mu\text{m}$ . For two groups to have means that are statistically different, the comparison intervals must not overlap. Except for the Global Icon-based implant, all implants, when studied under the same head contact condition, showed statistically significant differences between age groups in relation to the 20  $\mu\text{m}$  research variable. For the 50  $\mu\text{m}$  research variable, only the Sidus-based, Simpliciti-based, and SMR-based implants with no head contact showed statistically significant differences between age groups. The absence

of contact between the humeral head component and the bone surface impacted implants' performance, especially in the 60-80 age group.

## Discussion

The main finding of this study is that the age-induced decline in bone density may not pose a contraindication *per se* to stemless ATSA in elderly patients—even though bone-implant micromotions increased with age, some stemless shoulder implants showed good overall performance, even when assessed with the most conservative threshold for osseointegration (20  $\mu\text{m}$ ). For the less conversative osseointegration threshold (150  $\mu\text{m}$ ), all stemless implants presented good primary stability.

Except for the Global Icon-based implant, all implants showed statistically significant differences between age groups when an osseointegration threshold of 20  $\mu\text{m}$  was considered, highlighting the influence of bone density on primary stability—since the population under study proved to be statistically different only in terms of bone density, differences in results are caused by variations in density distributions alone. These findings are consistent with Levin et al<sup>25</sup>, who reported that age and low proximal humeral bone density are among the main reasons for switching to a stemmed implant. The assumption of a 50  $\mu\text{m}$  osseointegration threshold resulted in a substantial improvement in the performance of all stemless implants compared to the 20  $\mu\text{m}$  threshold, which underscores the sensitivity of primary stability to the osseointegration threshold, a point of controversy in the literature.<sup>22,14,31,38</sup> For the 50  $\mu\text{m}$  osseointegration threshold (Figure 4 (b)), micromotions were less dependent on bone density—only the Sidus-based, Simpliciti-based, and SMR-based implants with no head contact showed statistically significant differences between age groups. The overall limited influence of bone density on the results also suggests that the patients'

age may not hinder the application of a stemless design, which is in agreement with the findings of Baumgarten.<sup>3</sup> According to this author, an increased age does not appear to affect the clinical and radiographic outcomes of a stemless ATSA, when compared with a younger population. In this way, age may not be a contraindication to this procedure.

The Global Icon-based and Inhance-based implants had the best performance from the primary stability point of view. For the 20  $\mu$ m and 50  $\mu$ m research variables, these implants showed the lowest differences between age groups, being therefore the least sensitive to bone density. Quental et al<sup>31</sup> also reported a low impact of bone density on the Global Icon-based implant. For the 50  $\mu$ m osseointegration threshold, the Global Icon-based and Inhance-based implants consistently exhibited average surface areas either null or lower than 5%, which is likely of little concern, especially given the conditions of this study. The present study considers an immediate postoperative situation, where osseointegration has not yet occurred. As the osseointegration process evolves, stability is expected to increase, which should improve the implant's performance. Moreover, the loading conditions of the shoulder during the first few months after surgery are expected to be less intense than those considered in this study. In other words, the results presented are likely worst-case scenarios.<sup>5,31</sup>

When contact was considered between the humeral head component and the resected bone surface, the Simpliciti-based design had the worst performance. On the other hand, when no contact was considered, the Sidus-based implant presented the poorest performance. While the differences between these implants were not significant when head contact existed, they were significant in the absence of head contact. Therefore, considering both contact conditions and research variables, the Sidus-based implant seems to exhibit the least favorable overall performance.



In general, the presence of a collar covering the entire surface of the bone or, in its absence, the establishment of contact between the humeral head component and bone seems to contribute to primary stability, as also noted by Churchill and Athwal<sup>7</sup> and Quental et al<sup>31</sup>. This outcome was evidenced by the good performance of the Global Icon-based implant, which possesses a solid collar, as well as the performance of the other implants when contact between the humeral head component and bone was simulated. Among the implants that do not have a solid collar covering the entire bone surface, the Inhance-based implant proved to be the most insensitive to the contact condition between the humeral head component and bone. This could be an important feature, considering the practical challenge of ensuring optimal positioning of the humeral head component *in vivo*. Conversely, the Sidus-based design was shown to be the most sensitive to this positioning. The differences between implants, within each age group, were particularly noticeable when an osseointegration threshold of 20  $\mu\text{m}$  was considered. For an osseointegration threshold of 50  $\mu\text{m}$  the differences were less pronounced, although the Sidus-based implant with no humeral head contact continued to stand out negatively from the remaining designs. The overall impact of implant design on primary stability corroborates the infeasibility of extrapolating results between stemless implants, as underscored in the literature.<sup>7</sup>

The present study contains some limitations. Although the population considered in this study represents a major advance compared to those of other studies, which only considered one subject<sup>14,31</sup>, the conclusions drawn in this study can only be applied to it. Still, since the normality of the data was verified, the sample can be characterized as a representative group of the population. As far as the authors know, the population considered did not meet the criteria for ATSA, which means that bone changes that may occur as a consequence of the pathologies for which ATSA is indicated were not accounted for. The development of the FE models relied on assumptions and

simplifications that may not perfectly translate into clinical practice. For instance, bone was represented as an isotropic material, a simplification commonly accepted in existing literature due to limitations in extracting detailed information from medical imaging data, even though it may not fully capture its behavior.<sup>37,30</sup> Press-fit or other compression mechanisms were disregarded between the bone and implants. The simulation of press-fit would enhance contact between the bone and implant, likely decreasing interface micromotions. The coefficients of friction considered in this study were constant, i.e., they did not consider the possible variance associated with bone quality and condition. Therefore, the conclusions drawn from this study must be considered assuming that the factors influencing the friction coefficients were the same within the stemless implants.<sup>5,31</sup> This study examined five specific anatomic stemless shoulder implants and did not assess all commercially available options. Other designs may exhibit different performance characteristics. Moreover, the included stemless shoulder implants were modeled based on the information available in their respective technical guides. Consequently, geometric differences may exist between the developed computational models and the corresponding physical implants. Although the morphing of the different humerus geometries to a single geometry allowed limiting the differences between subjects to the density distribution alone, the applied procedure may have introduced minor inconsistencies in the morphed density distributions.<sup>2,39</sup>

## Conclusion

An age-related decrease in bone density led to increased micromotions in the developed finite element models, thereby influencing the primary stability of the five stemless shoulder implants evaluated. Nevertheless, age alone did not appear to be a contraindication for stemless anatomic

total shoulder arthroplasty. Regarding primary stability, the Global Icon-based and Inhance-based implants had the best performance and proved to be the least sensitive to bone density.

## References

1. Albers CGM, Chatindiara I, Moreno G, Poon PC. Good clinical and radiologic outcomes with the SMR Stemless anatomic TSA after a minimum of 2 years' followup. *Seminars in Arthroplasty JSES*. 2021 Sep 1;31(3):563–70. <https://doi.org/10.1053/j.sart.2021.03.006>
2. Bartenschlager S, Dankerl P, Chaudry O, Uder M, Engelke K. BMD accuracy errors specific to phantomless calibration of CT scans of the lumbar spine. *Bone*. 2022 Apr 1;157. <https://doi.org/10.1016/j.bone.2021.116304>
3. Baumgarten KM. Is stemless total shoulder arthroplasty indicated in elderly patients? *J Shoulder Elbow Surg*. 2023 Feb 1;32(2):260–8. <https://doi.org/10.1016/j.jse.2022.08.003>
4. Bergmann G, Damm P (ed. ). *OrthoLoad* . Julius Wolff Institute, Berlin Institute of Health at Charité Universitätsmedizin Berlin. 2008.
5. Berth A, März V, Wissel H, Awiszus F, Amthauer H, Lohmann CH. SPECT/CT demonstrates the osseointegrative response of a stemless shoulder prosthesis. *J Shoulder Elbow Surg*. 2016 Apr 1;25(4):e96–103. <https://doi.org/10.1016/j.jse.2015.09.009>
6. Brabston EW, Fehring E V., Owen MT, Ponce BA. Stemless Humeral Implants in Total Shoulder Arthroplasty. Vol. 28, *The Journal of the American Academy of Orthopaedic Surgeons*. NLM (Medline); 2020. p. e277–87. <https://doi.org/10.5435/JAAOS-D-16-00747>
7. Churchill RS, Athwal GS. Stemless shoulder arthroplasty—current results and designs. Vol. 9, *Current Reviews in Musculoskeletal Medicine*. Humana Press Inc.; 2016. p. 10–6. <https://doi.org/10.1007/s12178-016-9320-4>
8. Comenda M, Quental C, Folgado J, Sarmiento M, Monteiro J. Bone adaptation impact of stemless shoulder implants: a computational analysis. *J Shoulder Elbow Surg*. 2019 Oct 1;28(10):1886–96. <https://doi.org/10.1016/j.jse.2019.03.007>

9. Compston J. Bone Quality: What is it and How is it Measured? *Arq Bras Endocrinol Metab.* 2006;50(4):579–85. <https://doi.org/10.1590/s0004-27302006000400003>
10. DePuy Synthes. INHANCE™ SHOULDER SYSTEM - Surgical Technique. 2021.
11. DePuy Synthes. GLOBAL ICON™ Stemless Shoulder System - Surgical Technique. 2017.
12. Edgar H, Daneshvari Berry S, Moes E, Adolphi N, Bridges P, Nolte K. New Mexico Decedent Image Database. Office of the Medical Investigator, University of New Mexico. 2020. <https://doi.org/10.25827/5s8c-n515>
13. Edmonds A. Shoulder Arthroplasty. In: Saunders R, Astifidis R, Burke S, Higgins J, McClinton M, editors. *Hand and Upper Extremity Rehabilitation: A Practical Guide*. 4th ed. Elsevier Inc.; 2016. p. 283–90.
14. Favre P, Henderson AD. Prediction of stemless humeral implant micromotion during upper limb activities. *Clinical Biomechanics*. 2016 Jul 1;36:46–51. <https://doi.org/10.1016/j.clinbiomech.2016.05.003>
15. Favre P, Seebeck J, Thistlethwaite PAE, Obrist M, Steffens JG, Hopkins AR, et al. In vitro initial stability of a stemless humeral implant. *Clinical Biomechanics*. 2016 Feb 1;32:113–7. <https://doi.org/10.1016/j.clinbiomech.2015.12.004>
16. Fedorov A, Beichel R, Kalpathy-Cramer J, Finet J, Fillion-Robin JC, Pujol S, et al. 3D Slicer as an image computing platform for the Quantitative Imaging Network. *Magn Reson Imaging*. 2012 Nov;30(9):1323–41. <https://doi.org/10.1016/j.mri.2012.05.001>
17. Felsenberg D, Boonen S. The bone quality framework: Determinants of bone strength and their interrelationships, and implications for osteoporosis management. Vol. 27, *Clinical Therapeutics*. Excerpta Medica Inc.; 2005. p. 1–11. <https://doi.org/10.1016/j.clinthera.2004.12.020>
18. Grant JA, Bishop NE, Götzen N, Sprecher C, Honl M, Morlock MM. Artificial composite bone as a model of human trabecular bone: The implant-bone interface. *J Biomech*. 2007;40(5):1158–64. <https://doi.org/10.1016/j.jbiomech.2006.04.007>

19. Gupta S, Van Der Helm FCT, Van Keulen F. Stress analysis of cemented glenoid prostheses in Total Shoulder Arthroplasty. *J Biomech.* 2004 Nov;37(11):1777–86. <https://doi.org/10.1016/j.jbiomech.2004.02.001>
20. Hawi N, Magosch P, Tauber M, Lichtenberg S, Habermeyer P. Nine-year outcome after anatomic stemless shoulder prosthesis: clinical and radiologic results. *J Shoulder Elbow Surg.* 2017 Sep 1;26(9):1609–15. <https://doi.org/10.1016/j.jse.2017.02.017>
21. Heuberer PR, Brandl G, Pauzenberger L, Laky B, Kriegleder B, Anderl W. Radiological changes do not influence clinical mid-term outcome in stemless humeral head replacements with hollow screw fixation: A prospective radiological and clinical evaluation. *BMC Musculoskelet Disord.* 2018 Jan 22;19(1). <https://doi.org/10.1186/s12891-018-1945-6>
22. Hopkins AR, Hansen UN. Primary stability in Reversed-anatomy glenoid components. In: *Proceedings of the Institution of Mechanical Engineers, Part H: Journal of Engineering in Medicine.* 2009. p. 805–12. <https://doi.org/10.1243/09544119JEIM557>
23. J. W. Tukey. *The Collected Works of John W. Tukey.* Taylor and Francis; 1984.
24. Keller TS. Predicting the comprehensive mechanical behavior of bone. *J Biomech.* 1994;27(9):1159–68.
25. Levin JM, Rodriguez K, Polascik BA, Zeng S, Warren E, Rechenmacher A, et al. Simple preoperative radiographic and computed tomography measurements predict adequate bone quality for stemless total shoulder arthroplasty. *J Shoulder Elbow Surg.* 2022 Dec 1; <https://doi.org/10.1016/j.jse.2022.05.008>
26. Lima Corporate. SMR® Stemless - Surgical Technique. 2016. 2016.
27. Lima Corporate. SMR® Stemless - Brochure. 2016.
28. Marigi EM, Elahi MA, Cancio-Bello AM, Duquin TR, Sperling JW. Stemless anatomic total shoulder arthroplasty: surgical technique and review of the literature. *JSES Reviews, Reports, and Techniques.* 2022 Nov 1;2(4):442–50. <https://doi.org/10.1016/j.xrrt.2022.08.001>

29. Myronenko A, Song X. Point-Set Registration: Coherent Point Drift. 2009 May 15; <https://doi.org/10.1109/TPAMI.2010.46>
30. Pitocchi J, Wesseling M, van Lenthe GH, Pérez MA. Finite element analysis of custom shoulder implants provides accurate prediction of initial stability. *Mathematics*. 2020 Jul 1;8(7). <https://doi.org/10.3390/math8071113>
31. Quental C, Folgado J, Comenda M, Monteiro J, Sarmento M. Primary stability analysis of stemless shoulder implants. *Med Eng Phys*. 2020 Jul 1;81:22–9. <https://doi.org/10.1016/j.medengphy.2020.04.009>
32. Rancourt D, Shirazi-Adl A, Drouin G, Paiement G. Friction properties of the interface between porous-surfaced metals and tibial cancellous bone. *J Biomed Mater Res*. 1990 Nov 13;24(11):1503–19. <https://doi.org/10.1002/jbm.820241107>
33. Roosa SMM, Hurd AL, Xu H, Fuchs RK, Warden SJ. Age-related changes in proximal humerus bone health in healthy, white males. *Osteoporosis International*. 2012 Dec;23(12):2775–83. <https://doi.org/10.1007/s00198-012-1893-1>
34. Si H. TetGen, a delaunay-based quality tetrahedral mesh generator. *ACM Transactions on Mathematical Software*. 2015 Jan 1;41(2). <https://doi.org/10.1145/2629697>
35. Soltanmohammadi P, Tavakoli A, Langohr GDG, Athwal GS, Willing R. Structural analysis of hollow versus solid-stemmed shoulder implants of proximal humeri with different bone qualities. *Journal of Orthopaedic Research*. 2022 Mar 1;40(3):674–84. <https://doi.org/10.1002/jor.25076>
36. Spizer V, Ackerman MJ, Scherzinger AL, Whitlock D. The Visible Human Male: A Technical Report. *Journal of the American Medical Informatics Association*. 1996;3(2):118–30.
37. Taylor M, Prendergast PJ. Four decades of finite element analysis of orthopaedic devices: Where are we now and what are the opportunities? *J Biomech*. 2015 Mar 18;48(5):767–78. <https://doi.org/10.1016/j.jbiomech.2014.12.019>

38. Viceconti M, Pancanti A, Dotti M, Traina F, Cristofolini L. Effect of the initial implant fitting on the predicted secondary stability of a cementless stem. Vol. 42, Med. Biol. Eng. Comput. 2004. <https://doi.org/10.1007/BF02344635>
39. Winsor C, Li X, Qasim M, Henak CR, Pickhardt PJ, Ploeg H, et al. Evaluation of patient tissue selection methods for deriving equivalent density calibration for femoral bone quantitative CT analyses. Bone. 2021 Feb 1;143. <https://doi.org/10.1016/j.bone.2020.115759>
40. Wodarek J, Shields E. Stemless Total Shoulder: A Review of Biomechanical Fixation and Recent Results. J Shoulder Elb Arthroplast. 2021 Jan;5:247154922110084. <https://doi.org/10.1177/24715492211008408>
41. Wright. Tornier SIMPLICITI™ shoulder system - Surgical Technique. 2016.
42. Yushkevich PA, Piven J, Hazlett HC, Smith RG, Ho S, Gee JC, et al. User-guided 3D active contour segmentation of anatomical structures: Significantly improved efficiency and reliability. Neuroimage. 2006 Jul 1;31(3):1116–28. <https://doi.org/10.1016/j.neuroimage.2006.01.015>
43. Zdravkovic V, Kaufmann R, Neels A, Dommann A, Hofmann J, Jost B. Bone mineral density, mechanical properties, and trabecular orientation of cancellous bone within humeral heads affected by advanced shoulder arthropathy. Journal of Orthopaedic Research. 2020 Sep 1;38(9):1914–9. <https://doi.org/10.1002/jor.24633>
44. Zimmer, Inc. Zimmer Sidus™ Stem-Free Shoulder -Surgical Technique. 2012.

## Figure and Table Legends

**Figure 1** Anterior view of the 3D geometric models of the stemless shoulder arthroplasties. The green surfaces represent the coated or blasted regions of the implants, while the blue surfaces represent the non-treated regions. The surfaces of the humeral head component interacting with bone when contact is considered are depicted in red.

**Figure 2** Average cumulative distributions of the percentage of coated or blasted areas above a given micromotion for all stemless implants, considering the: (a) 20-40 age group, and (b) 60-80 age group. Normalization of the surface areas was performed with the total coated or blasted area of each implant, corresponding to 3401 mm<sup>2</sup> for the Global Icon-based implant, 1721 mm<sup>2</sup> for the Sidus-based implant, 1644 mm<sup>2</sup> for the Simpliciti-based implant, 2068 mm<sup>2</sup> for the SMR-based implant, and 2430 mm<sup>2</sup> for the Inhance-based implant. For each coordinate pair, the y-coordinate represents the average surface area, computed among all subjects in the respective age group, for which micromotions are equal to or greater than the micromotion given by the x-coordinate.

**Figure 3** Distribution of the average micromotions computed in the coated or blasted surfaces of the stemless implants for the 20-40 and 60-80 age groups: (a) Global Icon-based implant; (b) and (f) Sidus-based implant; (c) and (g) Simpliciti-based implant; (d) and (h) SMR-based implant; and (i) and (j) Inhance-based implant. The results presented in (b), (c), (d), and (e) were obtained considering head contact between the humeral head components and the resected surface of the humerus, whereas the results presented in (f), (g), (h), and (i) were obtained considering no contact existed.

**Figure 4** Multiple comparison tests performed for the five stemless implants under evaluation, considering the research variables defined with an osseointegration threshold of: (a) 20 µm, and (b) 50 µm. The mean value of each group is represented by a marker. The lines crossing the markers symbolize the respective comparison intervals, being dashed for the simulations with no head contact. For two groups to have means that are statistically different, the comparison intervals must not overlap.

**Figure S1** Average bone density distributions for the 20-40 and 60-80 age groups: (a) Cut view of the proximal part of the humerus, (b) Slice view, with the middle slice corresponding to the resection plane, at the anatomical neck level.

**Figure S2** Dispersion of results on the cumulative distributions of the percentage of coated or blasted areas above a given micromotion, normalized by the total coated or blasted area, for each stemless implant and age group. The solid and dashed lines represent the average of the 20-40 and 60-80 age groups, respectively. The orange and blue shading cover the area between the best- and worst-case scenarios for the 20-40 and 60-80 age groups, respectively. For the best case, average



condition, and worst case, the minimum, average, and maximum micromotions were calculated at each node, respectively, over the 10 subjects in each age group.

**Table I** Friction coefficients considered between bone and the stemless implants.<sup>8,18,27,31,32</sup>

**Table II** Characteristics of the selected population, depicted by age group. SD represents the standard deviation. Bone density represents the average density in the most proximal region of the humerus and below the resection plane, computed for each subject, and then for each age group.

**Table SI** *P* values for differences between the 20-40, 40-60, and 60-80 age groups in terms of bone density, height, weight, and BMI.

**Table I** Friction coefficients considered between bone and the stemless implants.<sup>8,18,27,31,32</sup>

Interaction with Bone	Coefficient of Friction
Trabecular titanium (SMR-based core)	2.20
Sintered titanium beads (Simpliciti-based nucleus)	0.53
Rough titanium coating (Sidus-based, Global Icon-based, and Inhance-based anchor)	0.60
Cobalt-chromium (Humeral head component, for contact simulations)	0.26
Titanium (Non-treated regions)	0.36

**Table II** Characteristics of the selected population, depicted by age group. SD represents the standard deviation. Bone density represents the average density in the most proximal region of the humerus and below the resection plane, computed for each subject, and then for each age group.

Age Group	Subjects	Men	Women	Age	Bone	Height	Weight	BMI
				(Years)	Density (g/cm <sup>3</sup> )	(cm)	(Kg)	(Kg/m <sup>2</sup> )
Mean ± SD								
20-40	10	5	5	28.0 ± 3.7	0.70 ± 0.08	174 ± 9	84.4 ± 17.5	28.4 ± 7.1
40-60	10	5	5	46.9 ± 6.5	0.56 ± 0.07	173 ± 7	72.6 ± 10.4	24.1 ± 3.4
60-80	10	5	5	66.7 ± 4.1	0.56 ± 0.05	170 ± 8	70.2 ± 13.6	24.8 ± 4.7

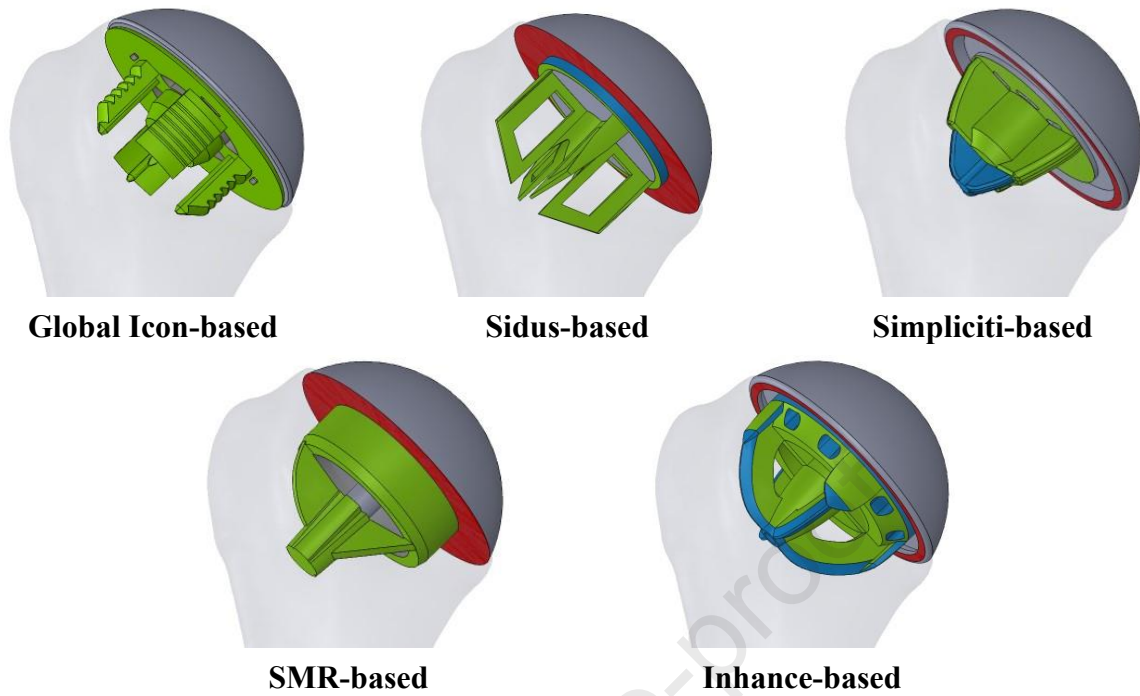
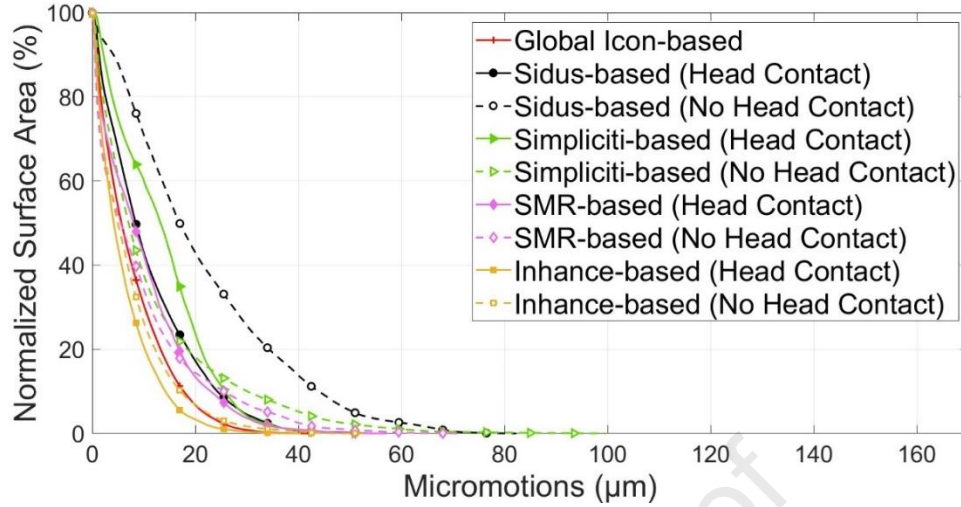
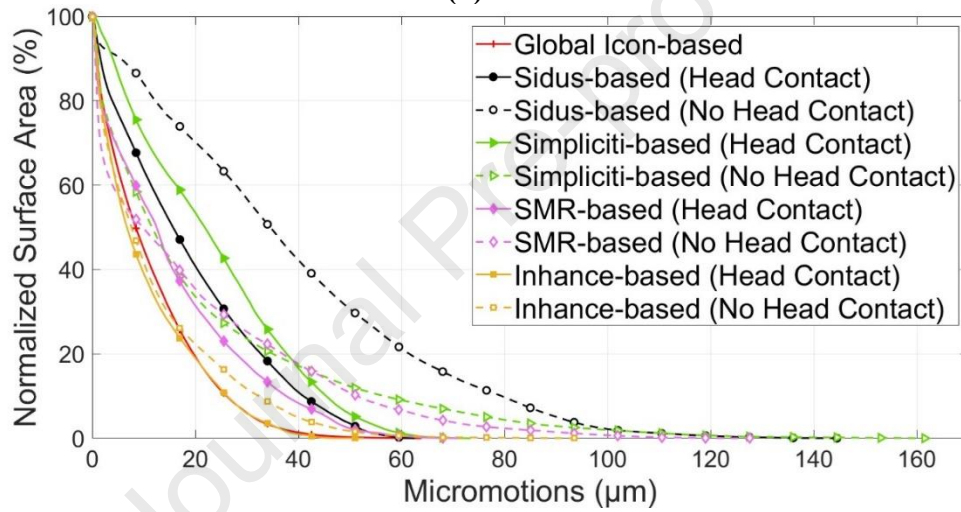


**Figure 1** Anterior view of the 3D geometric models of the stemless shoulder arthroplasties. The green surfaces represent the coated or blasted regions of the implants, while the blue surfaces represent the non-treated regions. The surfaces of the humeral head component interacting with bone when contact is considered are depicted in red.



(a)



(b)

**Figure 2** Average cumulative distributions of the percentage of coated or blasted areas above a given micromotion for all stemless implants, considering the: (a) 20-40 age group, and (b) 60-80 age group. Normalization of the surface areas was performed with the total coated or blasted area of each implant, corresponding to 3401 mm<sup>2</sup> for the Global Icon-based implant, 1721 mm<sup>2</sup> for the Sidus-based implant, 1644 mm<sup>2</sup> for the Simpliciti-based implant, 2068 mm<sup>2</sup> for the SMR-based implant, and 2430 mm<sup>2</sup> for the Inhance-based implant. For each coordinate pair, the y-coordinate represents the average surface area, computed among all subjects in the respective age group, for which micromotions are equal to or greater than the micromotion given by the x-coordinate.

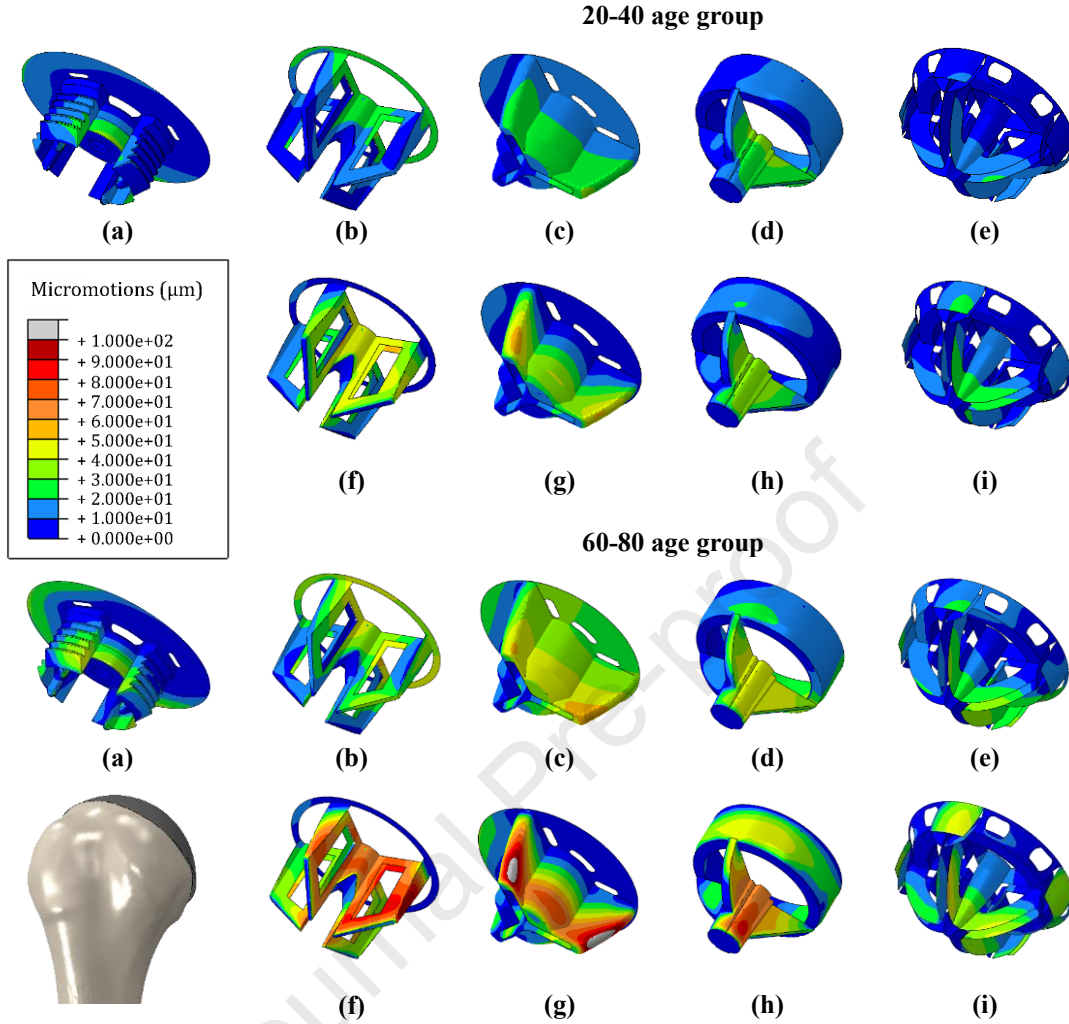
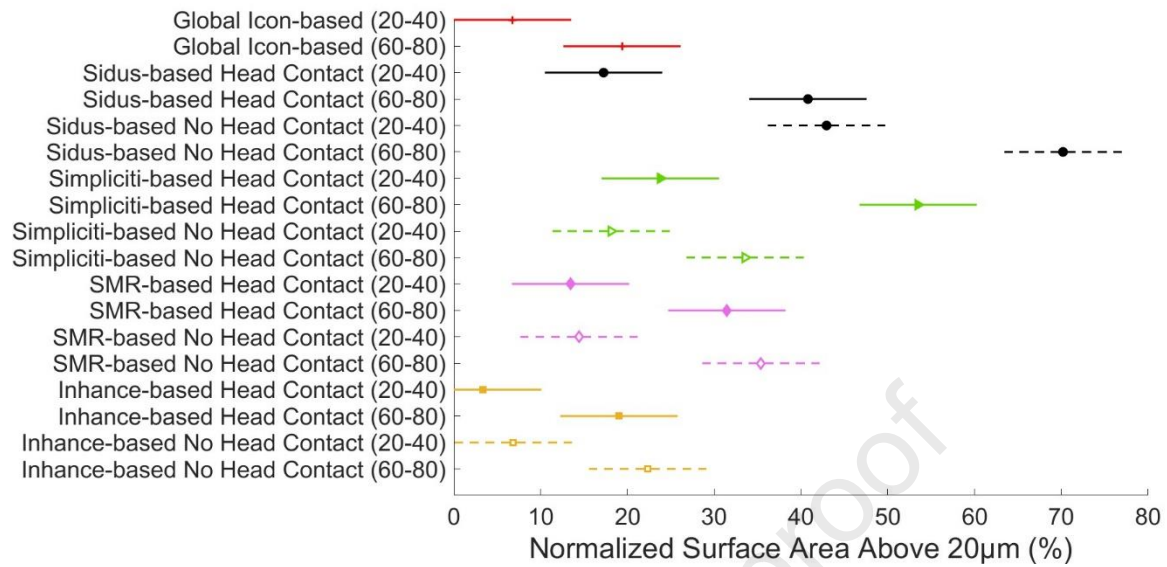
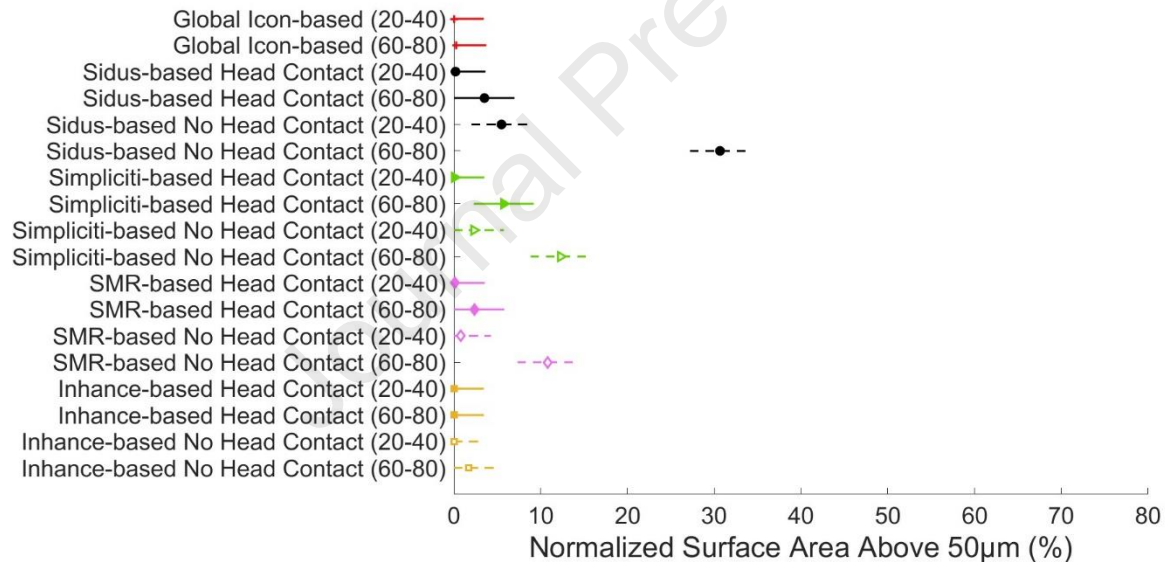


**Figure 3** Distribution of the average micromotions computed in the coated or blasted surfaces of the stemless implants for the 20-40 and 60-80 age groups: (a) Global Icon-based implant; (b) and (f) Sidus-based implant; (c) and (g) Simpliciti-based implant; (d) and (h) SMR-based implant; and (i) and (j) Inhance-based implant. The results presented in (b), (c), (d), and (e) were obtained considering head contact between the humeral head components and the resected surface of the humerus, whereas the results presented in (f), (g), (h), and (i) were obtained considering no contact existed.



(a)



(b)

**Figure 4** Multiple comparison tests performed for the five stemless implants under evaluation, considering the research variables defined with an osseointegration threshold of: (a) 20 µm, and (b) 50 µm. The mean value of each group is represented by a marker. The lines crossing the markers symbolize the respective comparison intervals, being dashed for the simulations with no head contact. For two groups to have means that are statistically different, the comparison intervals must not overlap.